An Accurate UAV 3-D Path Planning Method for Disaster Emergency Response Based on an Improved Multiobjective Swarm Intelligence Algorithm

Yuting Wan, *Student Member, IEEE*, Yanfei Zhong, *Senior Member, IEEE*, Ailong Ma, *Member, IEEE*, and Liangpei Zhang, *Fellow, IEEE*

***Abstract*—Planning a practical three-dimensional (3-D) flight path for unmanned aerial vehicles (UAVs) is a key challenge for the follow-up management and decision making in disaster emergency response. The ideal flight path is expected to balance the total flight path length and the terrain threat, to shorten the flight time and reduce the possibility of collision. However, in the traditional methods, the tradeoff between these concerns is difficult to achieve, and practical constraints are lacking in the optimized objective functions, which leads to inaccurate modeling. In addition, the traditional methods based on gradient optimization lack an accurate optimization capability in the complex multimodal objective space, resulting in a nonoptimal path. Thus, in this article, an accurate UAV 3-D path planning approach in accordance with an enhanced multiobjective swarm intelligence algorithm is proposed (APPMS). In the APPMS method, the path planning mission is converted into a multiobjective optimization task with multiple constraints, and the objectives based on the total flight path length and degree of terrain threat are simultaneously optimized. In addition, to obtain the optimal UAV 3-D flight path, an accurate swarm intelligence search approach based on improved ant colony optimization is introduced, which can improve the global and local search capabilities by using the preferred search direction and random neighborhood search mechanism. The effectiveness of the proposed APPMS method was demonstrated in three groups of simulated experiments with different degrees of terrain threat, and a real-data experiment with 3-D terrain data from an actual emergency situation.**

***Index Terms*—Ant colony optimization (ACO), multiobjective optimization, swarm intelligence, three-dimensional (3-D) terrain, unmanned aerial vehicle (UAV) path planning.**

Manuscript received January 28, 2022; revised April 19, 2022; accepted April 22, 2022. This work was supported by in part the National Natural Science Foundation of China under Grant 42071350 and Grant 42171336, and in part by the LIESMARS Special Research Funding. This brief was recommended by Associate Editor H. Takagi. *(Corresponding authors: Yanfei Zhong; Ailong Ma.)*

The authors are with the State Key Laboratory of Information Engineering in Surveying, Mapping and Remote Sensing and the Hubei Provincial Engineering Research Center of Natural Resources Remote Sensing Monitoring, Wuhan University, Wuhan 430079, China (e-mail: wanyuting@whu.edu.cn; zhongyanfei@whu.edu.cn; maailong007@whu.edu.cn; zlp62@whu.edu.cn).

Color versions of one or more figures in this article are available at https://doi.org/10.1109/TCYB.2022.3170580.

Digital Object Identifier 10.1109/TCYB.2022.3170580

I. Introduction

OVER the past decades, various natural disasters, such as floods and earthquakes, have caused great damage to human life and ecology. In the case of disasters, emergency response is particularly important. However, it can be difficult for emergency responders to enter the disaster area directly, due to the damage and the threat of further emergency events. As a new type of platform, unmanned aerial vehicles (UAVs) have been the subject of much attention, benefiting from the small size, low cost, and low environmental impact [1]–[3]. As a result, UAVs now play an important role in emergency news aerial photography, emergency rescue, and topographic mapping of post-disaster reconstruction. However, due to their unmanned nature, mission planning for UAVs is particularly important [4], [5]. Moreover, the path planning task is the most basic and important part of mission planning. A reasonable path plan helps the UAV to shorten the flight distance and avoid potential threats. As a result, path planning can improve the survival rate of UAVs in complex scenarios such as disaster emergency response [6], [7].

Although the two-dimensional (2-D) path search methods have achieved useful and practical results [8], [9], for the emergency response scenarios of natural disasters, such as tailings dam failure or debris flow, which are often located in remote mountainous areas, UAVs are faced with complex three-dimensional (3-D) terrain threats. Despite these challenges, 3-D environment-based path planning methods have been rapidly developed [10], [11]. Five categories of methods can be distinguished: 1) sampling-based approaches [12], such as the traditional Voronoi method [13], the rapidly exploring random trees (RRTs) method [14], [15], and RRT-star (RRT*) [16], [17]; 2) node-based methods, such as the A-star (A*) algorithm [18], harmony search [19], and the Dijkstra search approach [20]; 3) mathematical model-based methods, such as the mixed-integer programming (MIP) method [21] and the mixed-integer linear programming (MILP) method [22]; 4) evolutionary computation technology-based approaches, such as the genetic algorithm (GA) [23], [24]; and 5) multifusion methods [25], such as the geometrical path planning method [26].

As one of the most important branches of evolutionary computation, the particle swarm optimization (PSO) algorithm [27], [28] and ant colony optimization (ACO) algorithm [29], [30], which come from the swarm intelligence community, have also been used in 3-D path planning. Moreover, the planning methods referring to evolutionary computation omit the construction process of the complex path planning models, and the population-based global search capability can be employed to improve the global optimization capability [31], thus achieving the goal of stable convergence. In fact, because of the inherent NP completeness in the path planning task [32], this kind of problem can be solved using the effective heuristic methods, such as GAs [23], the PSO algorithm-based swarm intelligence methods [27], [28], and the differential evolution (DE) algorithm [33], [34], which can be used to effectively plan a path.

For the evolutionary computation technology-based methods for UAV 3-D path planning, the objective functions need to be constructed while also considering the actual environmental constraints as much as possible, so that different optimization strategies can then be designed. In the existing studies, the flight distance and the degree of terrain threat have usually been taken as the objective functions of the optimization, and the flight speed, acceleration, and fuel consumption have usually been taken as the constraint conditions [35]. Single-objective EA-based UAV 3-D path planning methods were first proposed. For example, Bayrak and Efe [36] proposed a field-programmable gate array (FPGA)-based offline 3-D UAV path planning approach through the use of a GA, where the total flight path length is taken as the objective function, and the flight mode and track point constraints are also considered. In addition, the genetic programming algorithm has also been introduced into UAV 3-D path planning [37]. Moreover, swarm intelligence methods have also been employed in UAV 3-D route planning. Blasi *et al.* [38] designed a hybrid probabilistic geometric strategy for optimal track recognition, referring to PSO through optimizing the minimum path length; and Huang *et al.* [39] combined ACO and the artificial potential field algorithm to obtain a dynamic path planning method by optimizing the cost functions of the dynamically changing threats.

However, in emergency response scenarios of natural disasters, only considering a single-objective function for the total flight path is not well suited to a real situation with the potential for physical collisions. The degree of the terrain threat posed by the physical obstacles should also be considered in the optimization model. Thus, multiobjective optimization evolutionary algorithm-based approaches have been employed. For example, Phung *et al.* [40] presented an enhanced swarm intelligence approach based on a discrete PSO method for UAV route planning by considering the coverage and obstacle avoidance; Adhikari *et al.* [41] designed a fuzzy adaptive swarm intelligence approach based on a DE algorithm for UAV path planning, where the mission is regarded as a multiobjective optimization process by minimizing the fuel, the degree of threat, and the path length; Yu *et al.* [42] proposed a constrained multiobjective DE for UAV path planning in disaster scenarios by considering the flight distance and risk; and Tong *et al.* [43] presented a multiobjective pigeon-inspired optimization method by considering the path length, path curvature, and path risk.

Furthermore, from the existing research into UAV 3-D path planning based on the evolutionary computation methods, it can be inferred that the objective function modeling and constraint setting are very important for practical 3-D path planning [40], [41]. However, with more factors considered in the objective functions, the objective space becomes more complex and multimodal. Furthermore, due to the difficulty of the complex practical path planning task, the original evolutionary computation methods lack local search capabilities, which hinders rapid convergence in local areas [44], [45]. Generally speaking, global and local optimization capabilities are two important factors to be considered in the evaluation of an algorithm [46]. Thus, the fact that the existing methods based on the original evolutionary computation methods lack local search capability can easily result in a nonoptimal 3-D path.

In this study, for the purpose of solving these concerns in the practical UAV 3-D path planning task for emergency response scenarios of natural disasters, an enhanced multiobjective swarm intelligence approach is presented for implementing accurate UAV 3-D path planning (APPMS). The innovations and contributions of this research are summarized as follows.

A. Accurate Multiobjective Framework for UAV 3-D Path Planning

The UAV 3-D route planning mission is transformed into a multiobjective optimization task with constraints, in which the objectives of the total flight path length and the degree of terrain threat based on the various flight constraints are accurately modeled to resolve the concerns of inaccurate flight path modeling. In addition, accurate optimization through an enhanced swarm intelligence approach is introduced to address the problem of the solution easily falling into a local extremum.

B. Accurate Modeling for UAV 3-D Path Planning

Due to the lack of consideration of the actual emergency flight constraints, the objective function modeling of the UAV 3-D path planning may be inaccurate, which can lead to a flight risk in actual emergency tasks. In the APPMS method, the objectives describing the total flight path length and the degree of terrain threat are accurately constructed with the corresponding constraints. In order to obtain closer to the actual emergency flight constraints, the function of the terrain threat degree is first improved, in which the ratio of the safe distance and the multidirectional distance between the flight path point and terrain edge is calculated. In addition, the safe flight distance and the horizontal and vertical turning angles are also constrained in the objective functions.

C. Global and Local Optimization-Based Search Strategy

As more factors are considered in the objective functions, the objective space becomes more complex and multimodal, and the existing methods based on evolutionary computation

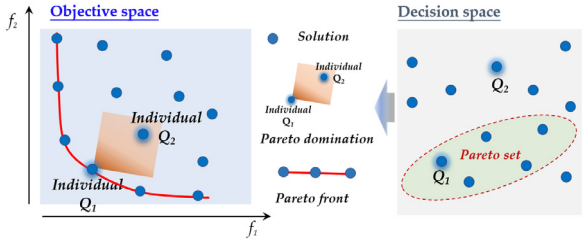

Fig. 1. Illustration of a multiobjective optimization problem, with Pareto domination and the Pareto front in objective space, and the Pareto set in decision space.

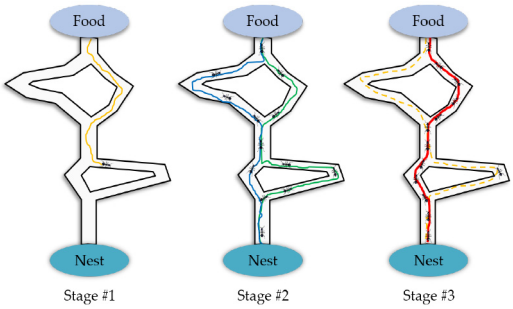

Fig. 2. ACO: A simulation optimization method that imitates the foraging behavior of ants from the nest to food. In stage #1, an ant finds the food and brings the news back to the nest. In stage #2, the ant colony travel from the nest to the food point along different paths, and release pheromones which are inversely proportional to the length of the foraging route. The ants can communicate with each other and learn the length of each path. In stage #3, after mutual communication, the ants will choose the path with the highest pheromone concentration, and the optimal route with the highest pheromone concentration is finally found.

lead to a nonoptimal search path, due to the lack of local optimization capability. In the proposed APPMS method, an accurate swarm intelligence search method based on improved ACO is introduced, which can improve the global search capability. In addition, for the purpose of evolving and refining the solutions, the preferred search direction and random neighborhood search mechanism are utilized to maintain a uniform distribution and the diversity of the Pareto solution set, and improve the local search capability, respectively.

The remainder of this article is organized as follows. Section II presents the related research background, including multiobjective optimization and ACO. The overall framework of the APPMS method is presented in Section III. Section IV describes the experiments and analyses. Finally, in Section V, we draw our conclusions.

II. Related Research Background

The UAV 3-D route planning mission can be considered as a constrained optimization problem [47]. Constraints, such as the angle of climb, turning left and right, and terrain constraints can be considered as part of the objective functions of the flight route distance and the degree of terrain threat [48].

The relevant research background is also introduced in this section, including the basic theory of the multiobjective optimization used to optimize the UAV 3-D path length and the degree of threat, and the ACO used to search for solutions.

A. Multiobjective Optimization

When a problem has a tradeoff solution set between several objectives, the multiple objective functions of the problem can be simultaneously optimized through the use of a multiobjective optimization method. An illustration of a multiobjective optimization problem is given in Fig. 1, and a basic description of a multiobjective optimization problem with p objectives is given as follows:

$$\begin{aligned} \text{minimize} \quad & F(\boldsymbol{Q}) = \{f_1(\boldsymbol{Q}), f_2(\boldsymbol{Q}), \ldots, f_p(\boldsymbol{Q})\} \\ \text{s.t.} \quad & \begin{cases} \boldsymbol{Q} = (q_1, q_2, \ldots, q_n)^T \\ r_i(\boldsymbol{Q}) \geq 0 (i = 1, 2, \ldots, m) \\ s_i(\boldsymbol{Q}) = 0 (i = 1, 2, \ldots, o) \end{cases} \end{aligned} \tag{1}$$

where $\boldsymbol{Q}$ is the solution variable, and $r_i(\boldsymbol{Q})$ and $s_i(\boldsymbol{Q})$ are the inequality and equality constraints, respectively. Therefore, when the solutions meet the constraints, they can be called "feasible solutions," and the others are "infeasible solutions," which do not participate in the optimization. In addition, in terms of the individual comparisons of the solutions, differing from the single-value comparison of a single-objective optimization task, multiple objectives values are taken into consideration, as shown in (2). When the solution individuals are satisfied, the solution individual $\boldsymbol{Q}_1$ Pareto dominates $\boldsymbol{Q}_2$

$$\begin{aligned} &\forall i = 1, 2, \ldots, p, f_i(\boldsymbol{Q}_1) \leq f_i(\boldsymbol{Q}_2) \\ &\quad \wedge \exists j = 1, 2, \ldots, p, f_j(\boldsymbol{Q}_1) < f_j(\boldsymbol{Q}_2). \end{aligned} \tag{2}$$

Therefore, differing from the single-objective optimization problem in which only one objective function value needs to be calculated and compared to finally obtain the optimal single solution, in the multiobjective optimization problem, a series of mutually nondominated solutions are finally obtained through the calculation and comparison of multiple objective function values. As shown in Fig. 1, the Pareto set and Pareto front are also defined. Multiobjective optimization has been successfully applied in planning and scheduling applications, such as job shop scheduling [49]–[52].

B. Ant Colony Optimization Approach

For the multiobjective optimization problem introduced above, it should be noted that the solutions need to be updated to converge to a satisfactory solution set. In particular, most of the practical optimization problems are NP-hard combinatorial optimization problems, and the objective space is extremely complex and multipeaked. As a result, a method with a strong search capability is urgently needed. Fortunately, the population-based evolutionary computation methods can provide an effective global search strategy. The ACO algorithm is briefly introduced here, an improved version of which is used in the proposed method.

As a representative swarm intelligence optimization approach, as presented in Fig. 2, the ACO method is a simulation-optimization algorithm that simulates the foraging behavior of ants. The ACO approach was first developed by Colorni *et al.* [53], and was used to solve the traveling salesman problem (TSP) [54]. Taking the TSP as an example, if

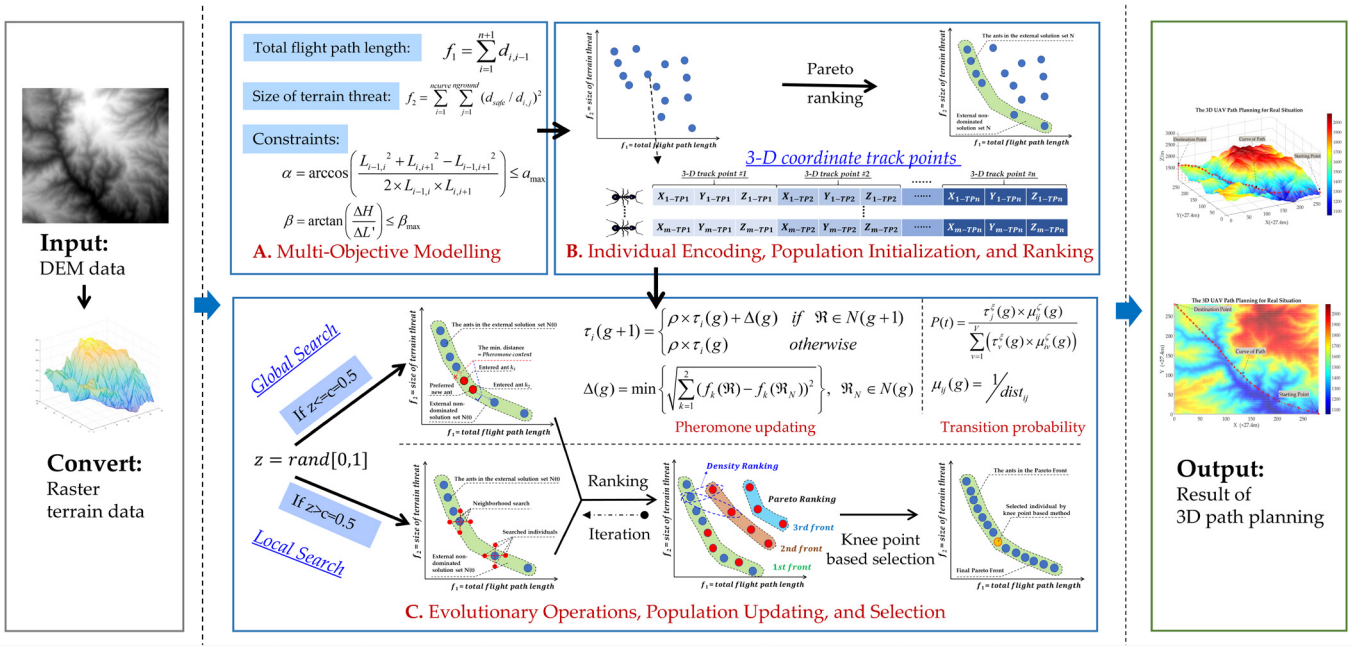

Fig. 3. Overall framework of the APPMS method for UAV path planning in a 3-D environment.

we assume that the quantity of cities is NC and the number of ants is NA, then at time ϑ, the transfer probability $P_{jk}^{i}(\vartheta)$ of the ith ant from city j to k is as shown in the following:

$$P_{jk}^{i}(\vartheta)=\begin{cases}\dfrac{\tau_{jk}^{\xi}(\vartheta)\times\mu_{jk}^{\zeta}(\vartheta)}{\sum_{v=1}^{\boldsymbol{V}_{\vartheta}}\left(\tau_{jv}^{\xi}(\vartheta)\times\mu_{jv}^{\zeta}(\vartheta)\right)}, & v\in\boldsymbol{V}_{\vartheta}\\ 0, & \text{otherwise}\end{cases}\tag{3}$$

where $j,k=1,2,\ldots,NC$, $i=1,2,\ldots,NA$, $\tau_{jk}^{\xi}(\vartheta)$ is the pheromone content between city j and city k, $\mu_{jk}^{\zeta}(\vartheta)$ is the heuristic information, and $\mu_{jk}^{\zeta}(\vartheta)=1/\text{dist}(j,k)$. $\text{dist}(j,k)$ indicates the distance between city j and city k. In addition, ξ and ζ are the heuristic factors, and $\boldsymbol{V}_{\vartheta}$ is the set of cities that have not been passed by the ith ant up until time ϑ.

Furthermore, it should be noted that the ants leave pheromones on every path they travel, which is extended to the ACO approach. For the purpose of preventing the individual solutions falling into locally optimal values, a pheromone volatilization mechanism is introduced, as shown in the following:

$$\tau_{jk}(\vartheta+1)=\dot{\lambda}\times\tau_{jk}(\vartheta)+\Delta\tau_{jk}(\vartheta)\tag{4}$$

$$\Delta\tau_{jk}(\vartheta)=\sum_{i=1}^{NA}\Delta\tau_{jk}^{i}(\vartheta)\tag{5}$$

where $\dot{\lambda}\in[0,1]$, which represents the volatilization coefficient; and $\Delta\tau_{jk}(\vartheta)$ denotes the objective function of the total crawling distance of the ith ant, and is the pheromones left by the ith ant on the path. Thus, benefiting from the idea of population-based global search, the ACO approach can be utilized to obtain the optimal solution in combinatorial optimization problems.

Algorithm 1 Pseudo Code of the APPMS Method

Input: DEM data converted into raster terrain data
/ Multi-objective modeling (6) and (7), constraints (8) and (9) */*
/ Individual encoding (X_{i-TPj}, Y_{i-TPj}, Z_{i-TPj}) */*
/ population initialization */*
Ranking for obtaining an external solution set N(0)
/ Main Loop */*
while $t < T_{max}$ **do**
  if $z \le c = 0.5$ **then** */* Conduct global search */*
    Calculate pheromone content (10)
    Calculate transition probability (12)
    Obtain preferred new ants to enter into new external solution set N(t)
  else */* Conduct local search */*
    Neighborhood search by random disturbance *randint*(1, 1, [−Φ, Φ])
  end if
  Calculation of the objective functions (6) and (7)
  Pareto ranking and density ranking
  $t = t + 1$
end while
Acquisition of the optimal solution by knee point based method
Output the final solution of the UAV planning path

III. Proposed APPMS Method

The framework of the proposed APPMS method is given in Fig. 3, in which there are three main steps: 1) multiobjective modeling of the total flight distance and the degree of terrain threat with constraints; 2) individual encoding, population initialization, and ranking for the initial paths; and 3) evolutionary operations, population updating, and selection for the searched 3-D paths. The pseudo code of the proposed APPMS method is given in Algorithm 1, and detailed descriptions of the main steps are presented in the following.

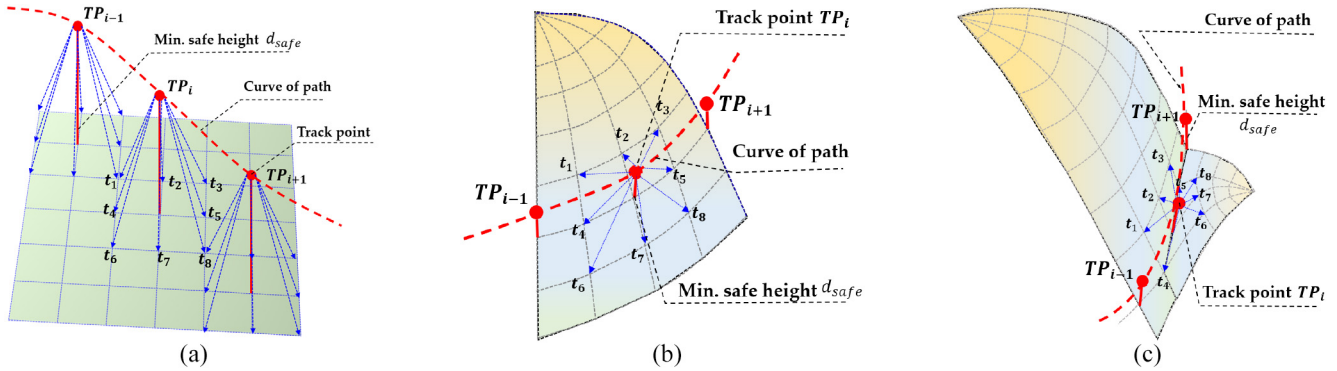

Fig. 4. Graphical illustration of a UAV flight path in 3-D terrain. (a) Track points in the planning path and calculation of the threat degree for flat terrain. (b) Calculation of the threat degree for single-sided mountainous terrain. (c) Calculation of the threat degree for two-sided mountainous terrain.

A. Multiobjective Modeling of the Total Flight Path Length and Degree of Terrain Threat With Constraints

In order to make the 3-D path of the UAV planning take into account both the total flight path length and the degree of terrain threat, two accurate objective functions for the 3-D path planning task are introduced, and the relevant constraints are given at the same time. As shown in Fig. 4, a graphical illustration of the UAV flight path in 3-D terrain and the calculation method for the threat factor is presented. The formulas are given in the following:

$$f_1 = \sum_{i=1}^{n+1} d_{i,i-1} \tag{6}$$

$$f_2 = \sum_{i=1}^{n} \sum_{j=1}^{n\_g} \left(d_{\text{safe}} / \Pi_{i,j}\right)^2 \tag{7}$$

where f_1 represents the functions of the total flight distance, f_2 denotes the degree of threat of the surrounding 3-D terrain, n is the number of the track points, $d_{i,i-1}$ denotes the distance between the ith and $i-1$th track points, and n_g is the number of discrete grid points on the edge of the terrain. As shown in Fig. 4, there are eight points $(t_1, t_2, \ldots, t_8)$ considered in the calculation. $\Pi_{i,j}$ denotes the distance between the ith discrete track point and the jth node on the terrain edge, and d_{safe} is the minimum safe distance between the UAV and the terrain edge.

Furthermore, in a real situation, if the turning angle is too large, it is considered not to be safe, and the UAV will not be allowed to fly. Thus, there are constraints on the horizontal and vertical turning angles, which are modeled in (8) and (9). A graphical illustration of the calculation of the turning angles is presented in Fig. 5

$$\alpha = \arccos\left(\frac{L_{i-1,i}^2 + L_{i,i+1}^2 - L_{i-1,i+1}^2}{2 \times L_{i-1,i} \times L_{i,i+1}}\right) \le a_{\max} \tag{8}$$

$$\beta = \arctan\left(\frac{\Delta H}{\Delta L'}\right) \le \beta_{\max} \tag{9}$$

where α represents the value of the horizontal turning angle, as shown in Fig. 5(a); $L_{i-1,i}$ denotes the length between the $i-1$th and the ith track points; $L_{i,i+1}$ and $L_{i-1,i+1}$ have the same meanings; and $a_{\max}$ is the maximum-allowable value for the horizontal turning angle (which was set to 75° in this study). β represents the value of the vertical turning angle, as shown in Fig. 5(b); ΔH denotes the value of the height difference between two track points; $\Delta L'$ represents the value of the horizontal projection distance between the two track points; and $\beta_{\max}$ is the maximum permissible value of the vertical turning angle (which was set to 60° in this study).

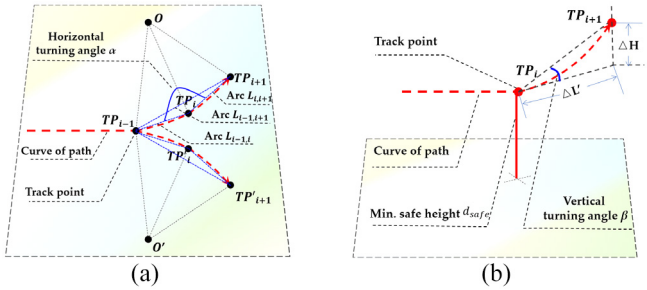

Fig. 5. Graphical illustration of calculation of the flight turning angle of the UAV. (a) Horizontal turning angle α. (b) Vertical turning angle β.

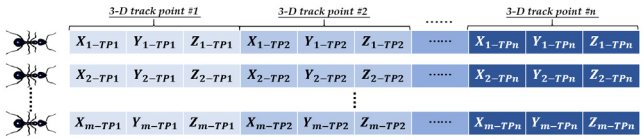

Fig. 6. Individual encoding and population initialization.

B. Evolutionary-Based Multiobjective Search

1) Individual Solution Encoding and Population Initialization: For the population-based evolutionary computation methods, the solutions representing the 3-D paths should be encoded into the individuals for the evolutionary generations. Specifically, for the improved swarm intelligence algorithm utilized for the UAV 3-D path planning task, the 3-D coordinate values of the track points are encoded into the individual solution. As presented in Fig. 6, an ant represents a planning path, where $(X_{i-TPj}, Y_{i-TPj}, Z_{i-TPj})$ represents the 3-D coordinates of the jth track point of the ith ant. Therefore, the number of trajectory points directly affects the dimension of individual solution, and too high dimension greatly affects the efficiency and accuracy of evolutionary

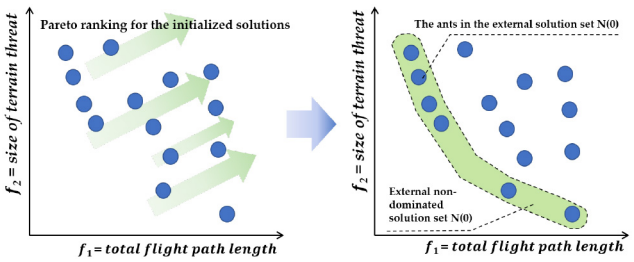

Fig. 7. Ranking for obtaining an external solution set.

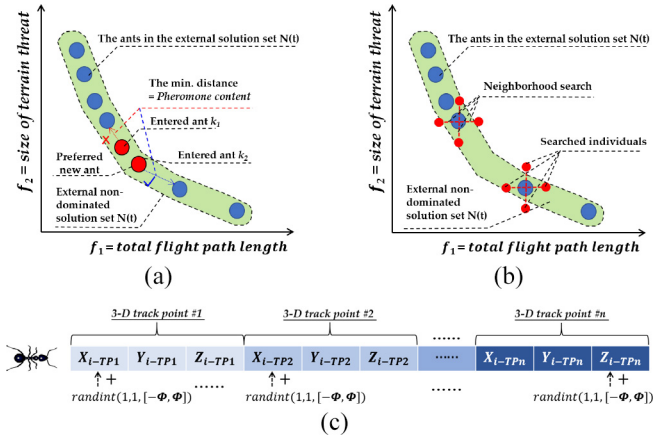

Fig. 8. Evolutionary search mechanism with global and local optimization and search capabilities. (a) Global optimization search, for the purpose of maintaining the uniform distribution and diversity of the Pareto optimal solution set. (b) Local search by introducing the random search strategy. (c) Calculation method for the local search.

search [55]. In this article, the suitable and same number of trajectory points are set in the compared multiobjective evolutionary algorithms.

In addition, m solution individuals are randomly initialized, simultaneously ranging from the smallest boundary value to the largest in a population. Those solution individuals in the population satisfying flight constraints (8) and (9) are considered as feasible solutions for the next iteration. The new solutions generated after this point also need to be restricted to obtain feasible and infeasible solutions.

2) Ranking for Obtaining External Solution Set: During the search process, in order to distinguish a good path from a bad path and save the current good individual solution, the current Pareto optimal individuals obtained by Pareto domination sorting are stored in an external solution set.

Therefore, in order to better guide the ants to search the feasible space for obtaining the optimal 3-D UAV flight path, in the multiobjective optimization problem, the external solution set $N(t)$ is constructed to store the Pareto optimal solution set obtained up to generation t. Thus, after the population initialization, the external solution set $N(0)$ is obtained by Pareto domination ranking, and is compared according to (2). Of course, before the Pareto ranking, the corresponding objective function values for all the ants in the population should be first calculated by (6) and (7). As shown in Fig. 7, six ants have entered into set $N(0)$, and they do not dominate each other.

3) Global and Local Search Joint Evolutionary Operations and Population Updating: After the initialization and ranking for obtaining the initial external solution set $N(0)$, evolutionary reproduction should be conducted to evolve the individuals in the population and obtain a better planning path. Moreover, to avoid the solutions falling into local extrema, an evolutionary search mechanism with global and local search capabilities is introduced.

First, for the global search, this aims to maintain the uniform distribution and diversity of the Pareto front, as shown in Fig. 8(a). There is an external nondominated solution set $N(t)$ in the t-th iteration, and if a new ant k enters this set, this indicates that this ant is nondominated. Thus, it should search for the location of the target space around it. However, when multiple ants enter $N(t)$, in order to achieve the purpose of this search stage, the minimum distance between the objective function values of the new ant k and the solution in set $N(t)$ is considered as the pheromone released by ant k at this time. The pheromone update process is shown in (10). When the distance is larger, the pheromone content is higher, which guides the other ants to search the ant's location domain with a higher probability, as shown in (12), which means there are preferred search directions based on the preferred new ant for obtaining a superior Pareto front

$$\tau_i(t+1) = \begin{cases} \rho \times \tau_i(t) + \nabla(t), & \text{if } \boldsymbol{X} \in N(t+1) \\ \rho \times \tau_i(t), & \text{otherwise} \end{cases} \tag{10}$$

$$\nabla(t) = \min \sqrt{\sum_{i=1}^{2} \left(f_i(\boldsymbol{X}) - f_i(\boldsymbol{X}_q)\right)} \boldsymbol{X}_q \in N(t) \tag{11}$$

where $\nabla(t)$ denotes the minimum distance described above, $\boldsymbol{X}$ represents a solution, and $f_i(\boldsymbol{X})$ and $f_i(\boldsymbol{X}_q)$ are the corresponding objective function values calculated by (6) and (7).

Furthermore, when the UAV is represented by the ant, the change of pheromone concentration on the flight path will directly affect the next route selected by the UAV, so the movement of the $k+1$th ant is related to the pheromone and distance of ant k. The ants with a high pheromone concentration and a close distance should take a higher probability as the next movement direction. The movement probability $P_{k+1\_k}(t)$ is shown in (12)

$$P_{k+1\_k}(t) = \frac{\tau_k^{\xi}(t) \times \mu_{k+1\_k}^{\zeta}(t)}{\sum_{v=1}^{m} \left(\tau_v^{\xi}(t) \times \mu_{k+1\_v}^{\zeta}(t)\right)} \tag{12}$$

where $\mu_{k+1\_k}^{\zeta}(t) = 1/d_{k+1\_k}$ and d_{k+1_k} represents the actual distance between the $k+1$th and the kth ants.

After the global search, in order to avoid the individual solutions falling into local minima, and accelerate the convergence to the global optimal solution, local search is conducted. A random number mechanism is introduced in this article, where, given a constant $c = 0.5$, if $z \le c$, the above global operation is performed. If $z > c$, a solution in $N(t)$ is selected as the next movement direction and its neighborhood is searched, as presented in Fig. 8(b). Moreover, the implementation method for the local search is given in Fig. 8(c), where a random

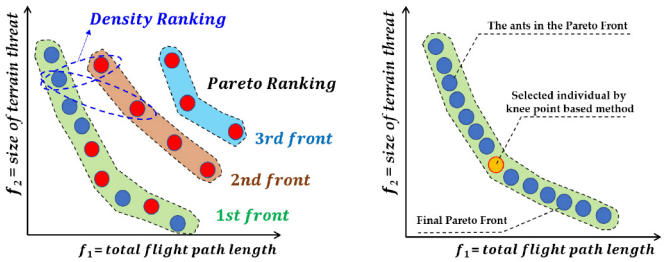

Fig. 9. Population ranking and updating, and the selection for the final output solution. (a) Pareto ranking and density ranking for maintaining the population size. (b) Knee point-based approach for selecting the final output solution individual from the final Pareto front.

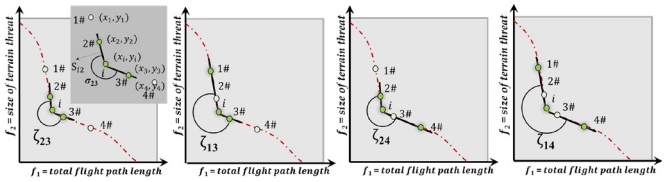

Fig. 10. Calculation method for the knee point-based selection method.

disturbance randint(1, 1, $[-\Phi, \Phi]$) is conducted on the 3-D coordinate values for the selected solution individual.

After the evolutionary reproduction, for the purpose of keeping the population size constant, ranking should be conducted. Pareto ranking and density ranking are both utilized [56], where the former is used to obtain the fronts with different serial numbers. However, in general, the first front is less than or more than the population size, so that density ranking is utilized, and the solution individual with a larger value of density is selected to enter the next iteration, as shown in Fig. 9(a).

C. Acquisition of the Optimal Path Plan and Selection of the Solution Individuals

The evolutionary operations and population updating are repeated until the number of search iterations reaches the maximum number $T_{\max}$ set artificially. The final Pareto front, that is, the Pareto optimal solution set, is then obtained.

For the Pareto optimal solution set obtained by multiobjective sorting, it can be found that a small disturbance in one objective can lead to a drastic change in another objective. Therefore, the inflection point on the Pareto frontier is often regarded as the optimal solution [57], [58]. A knee point-based method is therefore applied to select the final output solution individual from the final Pareto optimal solution set, as presented in Fig. 9(b). The calculation method is given in Fig. 10, where, for the ith solution in the Pareto optimal solution set, the angle ζ_i can be calculated by $\zeta_i = \max(\zeta_{23}, \zeta_{13}, \zeta_{24}, \zeta_{14})$ while considering the four individual neighborhood solutions. For example, the corresponding objective function values of the five individuals in the objective space are (x_1, y_1), (x_2, y_2), (x_i, y_i), (x_3, y_3), and (x_4, y_4), respectively. The distance is calculated by $S_{i2} = \sqrt{(x_i - x_2)^2 + (y_i - y_2)^2}$, and the distances between the other solutions are calculated in the same way. Thus, the angle σ_{23} is then calculated by $\sigma_{23} = \arccos((S_{i2}^2 + S_{i3}^2 - S_{23}^2)/2 \times S_{i2} \times S_{i3})$, and the other angles are calculated in the same way. This calculation is utilized for each solution individual, to obtain a set ζ, and the final optimal solution individual for optimal 3-D path planning can then be selected by $\max(\zeta)$.

IV. Experiments and Analyses

In order to verify the effectiveness of the proposed APPMS method, the traditional 3-D path planning method of A* [9], the nondominated sorting GA II (NSGA-II) [5], the multiobjective evolutionary algorithm based on decomposition (MOEA/D) [59], and the nondominated sorting GA III (NSGA-III) [60] were used for the comparison. For the multiobjective optimization methods, we carried out five repeated experiments, and compared the results using the mean and standard deviation. Moreover, three simulated digital terrain datasets and a real digital elevation model (DEM) dataset were utilized as the experimental datasets.

A. Experimental Datasets and Measures

1) Simulated Experimental Datasets: Three cases were constructed from simulated digital terrain. The original digital terrain was constructed using (13), and is shown in Fig. 11(a)

$$z_1(x, y) = \sin(y + \omega) + \kappa \sin(x) + \rho \cos\left(\psi\sqrt{y^2 + x^2}\right) + \phi \sin\left(\phi\sqrt{y^2 + x^2}\right) + \varpi \cos(y) \tag{13}$$

where x and y denote the abscissa and ordinate of a point on the horizontal plane; $z_1(x, y)$ denotes the corresponding terrain height; and ω, κ, ρ, ψ, ϕ, and ϖ are the terrain coefficients, which can simulate different topographic features.

In addition, in the flight process, there are usually various threats, such as mountain peaks or enemy defense areas. To facilitate the flight path planning, the equivalent mountain terrain was included in the planning model, as shown in (14)

$$z_2(x, y) = \sum_{i=1}^{k} H(i) \times \exp\left(-(x - X_c(i))^2/X_t(i) - (y - Y_c(i))^2/Y_t(i)\right) \tag{14}$$

where $z_2(x, y)$ denotes the corresponding mountain height; k is the number of the mountains; $H(i)$ corresponds to the height of the ith peak; $X_c(i)$ and $Y_c(i)$ denote the horizontal and vertical coordinates of the center of the ith peak on the horizontal plane; and $X_t(i)$ and $Y_t(i)$ denote the contour parameters of the ith peak. Thus, we can merge the threat equivalent terrain and the original digital terrain to form the equivalent digital terrain, as shown in (15)

$$z(x, y) = \max(z_1(x, y), z_2(x, y)). \tag{15}$$

The terrain coefficients were set to $\omega = 3 \times \pi$, $\kappa = 1/10$, $\rho = 9/10$, $\psi = 1/2$, $\phi = 1/2$, and $\varpi = 3/10$. The other corresponding parameters in the three simulated cases are given

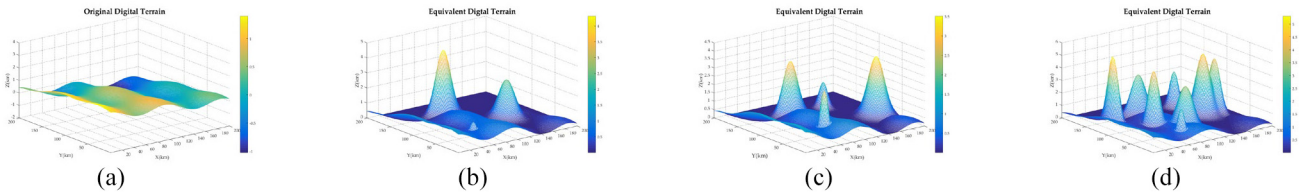

Fig. 11. Original digital terrain and the equivalent digital terrain for the simulated datasets. (a) Original digital terrain. (b) Equivalent digital terrain _3 threats. (c) Equivalent digital terrain _4 threats. (d) Equivalent digital terrain _8 threats.

TABLE I
PARAMETER SETTINGS FOR THE THREE SIMULATED DATASETS

	#	(x_c, y_c) (km)	(x_t, y_t) (km)	H (km)
Three threats	1	(45, 60)	(80, 50)	1.0
	2	(90, 150)	(290, 220)	2.5
	3	(150, 90)	(120, 260)	4.3
Four threats	1	(50, 70)	(80, 50)	2.6
	2	(80, 180)	(300, 220)	3.5
	3	(150, 90)	(120, 250)	3.2
	4	(150, 145)	(90, 60)	1.5
Eight threats	1	(30, 70)	(80, 50)	2.3
	2	(60, 100)	(300, 220)	3.4
	3	(150, 90)	(120, 250)	3.2
	4	(100, 160)	(250, 160)	4.8
	5	(140, 40)	(200, 50)	5.3
	6	(100, 180)	(230, 50)	3.8
	7	(90, 70)	(150, 100)	4.5
	8	(150, 150)	(90, 60)	2.8

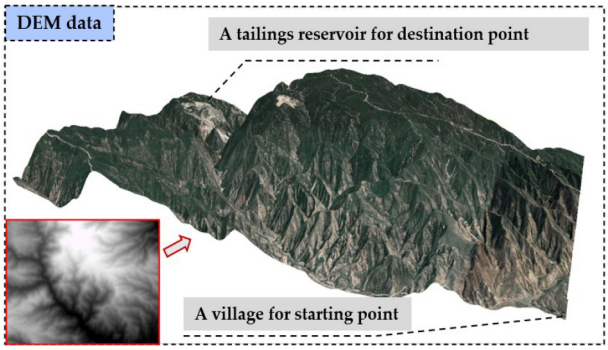

Fig. 12. Illustration of the real-data experimental dataset.

in Table I. The three cases of simulated digital terrain are presented in Fig. 11(b)–(d).

2) Real-Data Experimental Dataset: For the real data, a dam break emergency response scenario in a mining area was considered, for which the DEM data around the mining area were utilized, the size is 280 × 280, the spatial resolution is 27.4 m, and the elevation range is 1056–2086 m as shown in Fig. 12.

3) Measures for the Results: In addition to visually judge the superiority of the path planning for the UAV, for the multiobjective UAV 3-D path planning methods, a variety of indicators were used to evaluate the superiority of the searched Pareto front, that is, the hypervolume (HV) [61], the pure diversity (PD) [62], and the spacing (S) [63], as shown in (16)–(18). In addition, it is to be expected that HV and PD are larger while S is smaller

$$HV = \text{hypervolume}\left(\bigcup_{i=1}^{|PF|} G_i\right) \tag{16}$$

$$PD(\boldsymbol{G}) = \max_{g_i \in \boldsymbol{G}}(PD(\boldsymbol{G} - g_i) + \text{diss}(g_i, \boldsymbol{G} - g_i))$$

$$\text{diss}(g, \boldsymbol{G}) = \max_{g_i \in \boldsymbol{G}}(\text{dissimilarity}(g, g_i)) \tag{17}$$

$$S = \text{std}(\min(\text{Dist}_{\text{matrix}}, [\ ], 2))$$

$$\text{Dist}_{\text{matrix}} = pair\_dist2(PF, PF) \tag{18}$$

where G_i represents the solutions in the Pareto optimal solution set. When calculating the HV, the values of the multiple objective functions are first normalized, and point [1, 1] is then selected as the reference point. $\text{diss}(g_i, \boldsymbol{G} - g_i)$ denotes the dissimilarity between g_i to a community $\boldsymbol{G}$. $\text{Dist}_{\text{matrix}}$ is the matrix obtained by calculating the Euclidean distance between two paired solutions. $\text{std}(\min(\text{Dist}_{\text{matrix}}, [\ ], 2))$ represents the standard deviation after the vector is made up of the minimum value in each column.

B. Simulated Experimental Results and Analyses

Three groups of simulated digital terrain were considered. The safe height was set to 200 m, and there were 100 3-D track points to search. In addition, for the multiobjective optimization-based methods, the number of iterations was set to 200, the population size was set to 20, and the mutation probability and crossover probability were set to 0.5 and 0.9, respectively. The experimental results are presented in Figs. 13–15. First, from the visual perspective, for the results of the simulated experiment with three threats, as presented in Fig. 13, it is clear that the path in the region R_{S3_1} for the traditional method of A* is worse than the paths in regions R_{S3_2}, R_{S3_3}, R_{S3_4}, and R_{S3_5} for NSGA-II, MOEA/D, NSGA-III, and the proposed APPMS method, and there is an obvious turn error. In addition, from the comparison of the main regions of R_{S3_2}, R_{S3_3}, and R_{S3_4}, it is clear that the APPMS method can obtain a better path than NSGA-II, MOEA/D, and NSGA-III, with the shortest flight length and the lowest risk.

For the simulated experimental results shown in Fig. 14, it can be found that there is an obvious collision risk in region R_{S4_1} with the A* method. However, from the comparison of the main regions of R_{S4_2}, R_{S4_3}, R_{S4_4}, and R_{S4_5}, it is apparent that the three methods of NSGA-II, MOEA/D, and NSGA-III are comparable, while the proposed APPMS method obtains a preferable path. In addition, for the simulated experiment with eight threats, as shown in Fig. 15, it can be first found that the traditional A* method has an obvious

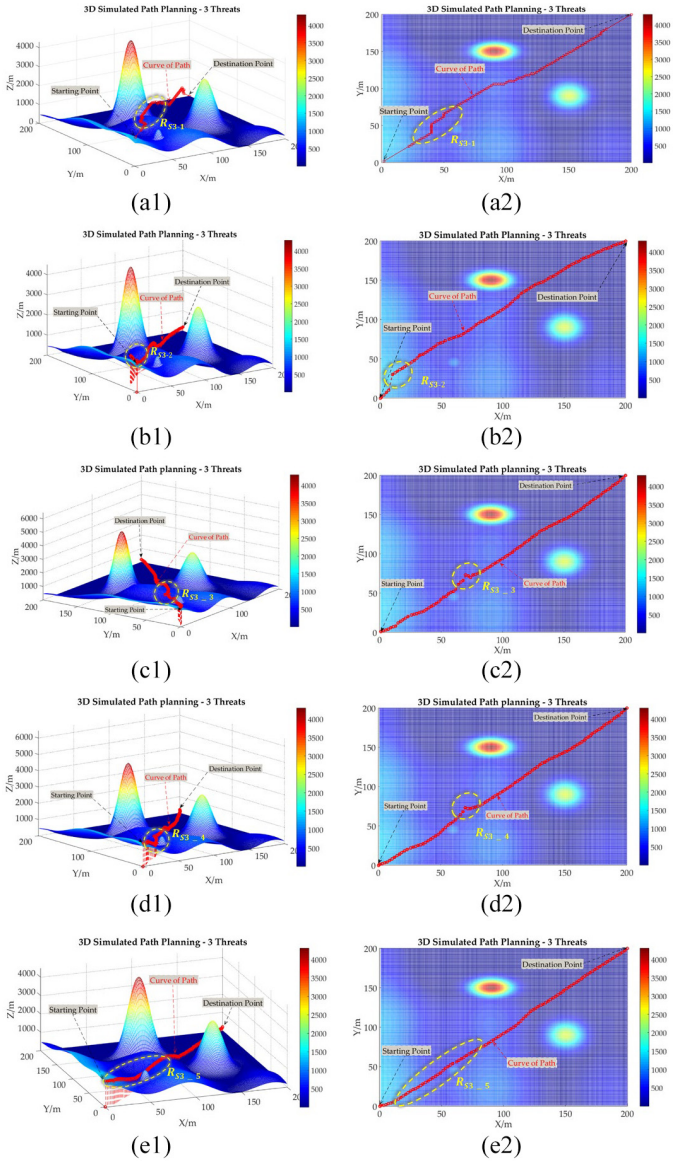

Fig. 13. Results of the simulated experiment with three threats. (a1) A*_three threats. (a2) Top view: A*. (b1) NSGA-II_three threats. (b2) Top view: NSGA-II. (c1) MOEA/D_three threats. (c2) Top view: MOEA/D. (d1) NSGA-III_three threats. (d2) Top view: NSGA-III. (e1) APPMS_three threats. (e2) Top view: APPMS.

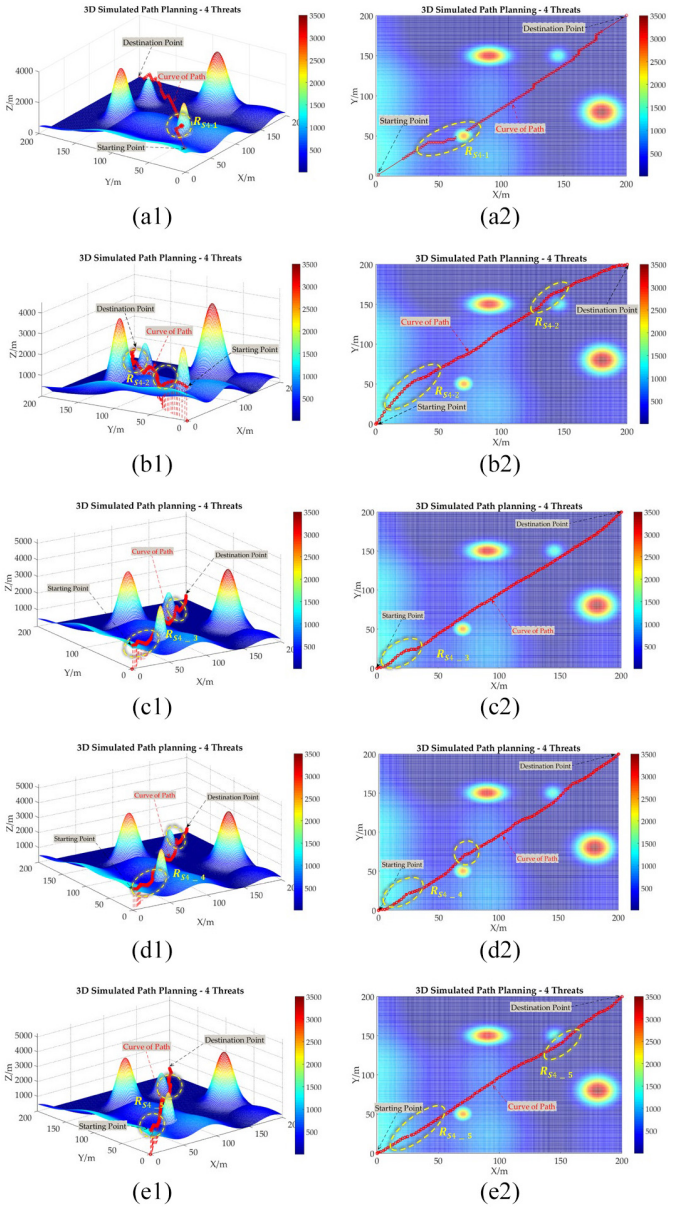

Fig. 14. Results of the simulated experiment with four threats. (a1) A*_four threats. (a2) Top view: A*. (b1) NSGA-II_four threats. (b2) Top view: NSGA-II. (c1) MOEA/D_four threats. (c2) Top view: MOEA/D. (d1) NSGA-III_four threats. (d2) Top view: NSGA-III. (e1) APPMS_four threats. (e2) Top view: APPMS.

turn error in region R_{S8_1}, and from the comparison of the main regions of R_{S8_2}, R_{S8_3}, R_{S8_4}, and R_{S8_5}, it is apparent that the proposed APPMS method achieves a smoother path than the other multiobjective optimization methods of NSGA-II, MOEA/D, and NSGA-III. Thus, it can be concluded that the traditional A* method may not be suitable in actual 3-D terrain, due to the longer path and the greater risk of collision. From a visual perspective, the three groups of simulated experimental results show that the proposed APPMS method can achieve preferable paths in different scenarios.

For the purpose of allowing a more intuitive comparison of the multiobjective optimization-based methods, the final Pareto fronts obtained by the proposed APPMS method and the NSGA-II, MOEA/D, and NSGA-III methods are presented in Fig. 17(a)–(c). It can be found that the APPMS method obtains a higher-quality Pareto front than the other methods. In addition, a quantitative evaluation of the Pareto fronts was also conducted, and the multiobjective indicators of HV, PD, and S were calculated. The quantitative results are presented in Table II. It is worth noting that the proposed method shows a superior performance in all the metrics for the eight-threat scenario. In addition, the proposed APPMS method also obtains first or second place for the three- and four-threat scenarios. The proposed method considers more superior and practical constraints, and makes comprehensive use of the global and local search capabilities to effectively improve the optimization ability of the optimization algorithm in the multidimensional and multimodal objective space. Therefore,

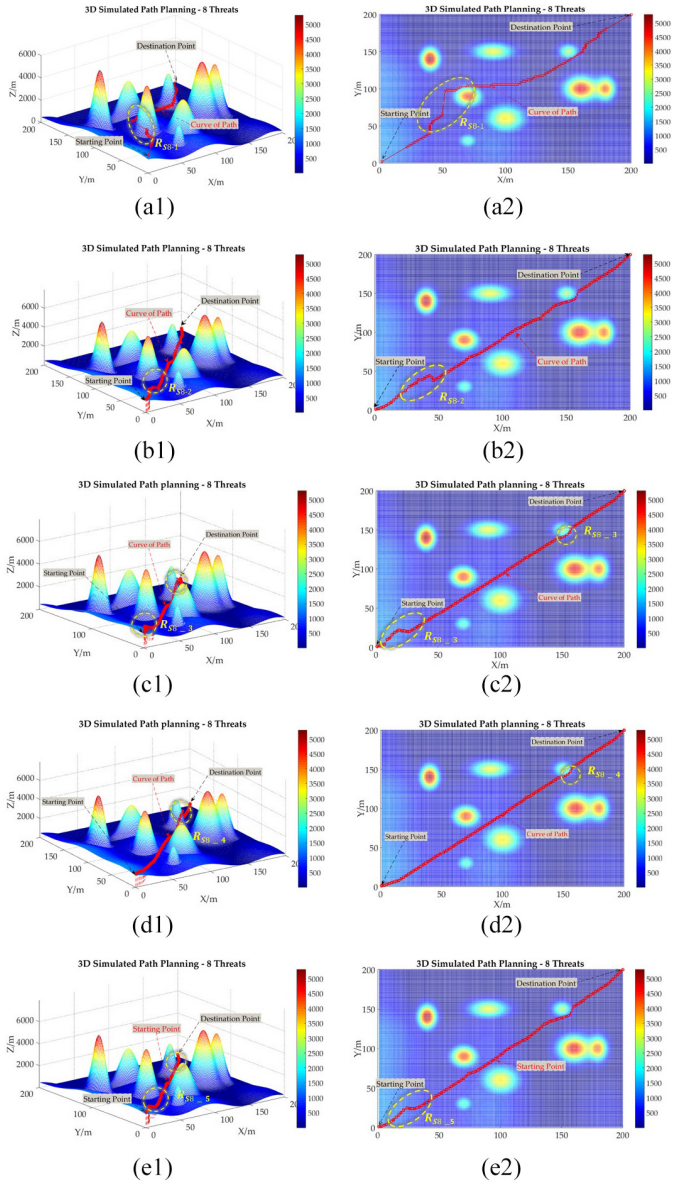

Fig. 15. Results of the simulated experiment with eight threats. (a1) A*_eight threats. (a2) Top view: A*. (b1) NSGA-II_eight threats. (b2) Top view: NSGA-II. (c1) MOEA/D_eight threats. (c2) Top view: MOEA/D. (d1) NSGA-III_eight threats. (d2) Top view: NSGA-III. (e1) APPMS_eight threats. (e2) Top view: APPMS.

in the optimization of multiobjective UAV 3-D path planning, the Pareto front obtained by the proposed method has better HV, PD, and S values. Overall, from these qualitative and quantitative results, the superior optimization ability of the proposed APPMS method has been proved.

C. Real-Data Experimental Results and Analyses

For the real-data experiment for a UAV 3-D flight mission, real DEM data for a simulated emergency response task were utilized, as shown in Fig. 12. The safe height was again set to 200 m for the multiobjective optimization-based methods, there were 36 3-D track points to search, the number of iterations was set to 200, the population size was set to 30, and the mutation probability and crossover probability were set to 0.5 and 0.9, respectively. The results of this real situation are given in Fig. 16.

TABLE II
MULTIOBJECTIVE INDICATORS FOR THE THREE SIMULATED EXPERIMENTS

#	Method	Metric		
		HV ↑	PD ↑	S ↓
Three threats	NSGA-II	0.5501 ± 0.0074	1.2080E3 ± 17.982	0.0399 ± 0.0018
	MOEA/D	0.6062 ± 0.0251	**1.3612E3** ± 35.138	0.0368 ± 0.0010
	NSGA-III	0.6779 ± 0.0214	1.1071E3 ± 38.930	0.0514 ± 0.0012
	APPMS	**0.6992** ± 0.0189	1.0262E3 ± 85.561	**0.0327** ± 0.0013
Four threats	NSGA-II	0.5510 ± 0.0213	1.1147E3 ± 87.836	0.0439 ± 0.0041
	MOEA/D	**0.7639** ± 0.0285	0.8099E3 ± 29.137	0.0568 ± 0.0031
	NSGA-III	0.7240 ± 0.0185	1.1965E3 ± 24.515	**0.0326** ± 0.0026
	APPMS	0.7378 ± 0.0185	**1.4271E3** ± 31.428	0.0674 ± 0.0033
Eight threats	NSGA-II	0.5936 ± 0.0138	1.3568E3 ± 39.537	0.0500 ± 0.0019
	MOEA/D	0.7017 ± 0.0093	1.2147E3 ± 59.159	0.0467 ± 0.0022
	NSGA-III	0.7261 ± 0.0165	1.0796E3 ± 51.122	0.0539 ± 0.0019
	APPMS	**0.8136** ± 0.0109	**1.3586E3** ± 22.679	**0.0446** ± 0.0020

TABLE III
MULTIOBJECTIVE INDICATORS FOR THE REAL-DATA EXPERIMENT

	Method	Metric		
		HV ↑	PD ↑	S ↓
Real	NSGA-II	0.5594 ± 0.0173	1.2271E3 ± 28.818	0.0216 ± 0.0014
	MOEA/D	0.5573 ± 0.0164	1.1280E3 ± 31.911	0.0268 ± 0.0009
	NSGA-III	0.6185 ± 0.0276	1.0312E3 ± 38.121	0.0276 ± 0.0014
	APPMS	**0.6331** ± 0.0148	**1.5163E3** ± 30.323	**0.0204** ± 0.0008

First, for the result of the traditional A* method, due to the lack of corresponding flight restrictions, and the fact that it only takes the shortest path as the objective function, there is a risk from excessive wind and power consumption during the flight, and there is also a collision risk, due to the lack of consideration of the turning angle and other factors. Thus, the A* method obtains poor results in region R_{r_1}. In addition, from the comparison of the main regions of R_{r_2}, R_{r_3}, and R_{r_4}, it can be seen that the three methods of NSGA-II, MOEA/D, and NSGA-III are comparable, which indicates that there is little difference between the three methods in the actual 3-D path planning task. From region R_{r_5}, it can be found that the proposed APPMS method obtains a preferable visual result, due to the tortuous paths in the results of the NSGA-II, MOEA/D, and NSGA-III methods, where the route length is too long and the risk degree is increased. In summary, the traditional A* method is not suitable for use in real 3-D terrain, due to the longer path and greater risk of collision and, from the visual perspective, the proposed APPMS method can obtain a preferable flight path, compared to NSGA-II, MOEA/D, and NSGA-III.

As in the simulated experiments with different threats, an intuitive comparison of the real-data experiment by the final Pareto fronts and a quantitative evaluation by the multiobjective indicators of HV, PD, and S are presented in Fig. 17(d) and Table III, respectively. From these results, it can be found that the novel APPMS method obtains a superior path planning performance, compared to NSGA-II, MOEA/D, and NSGA-III. The proposed APPMS method benefits from the comprehensive utilization of the global and local

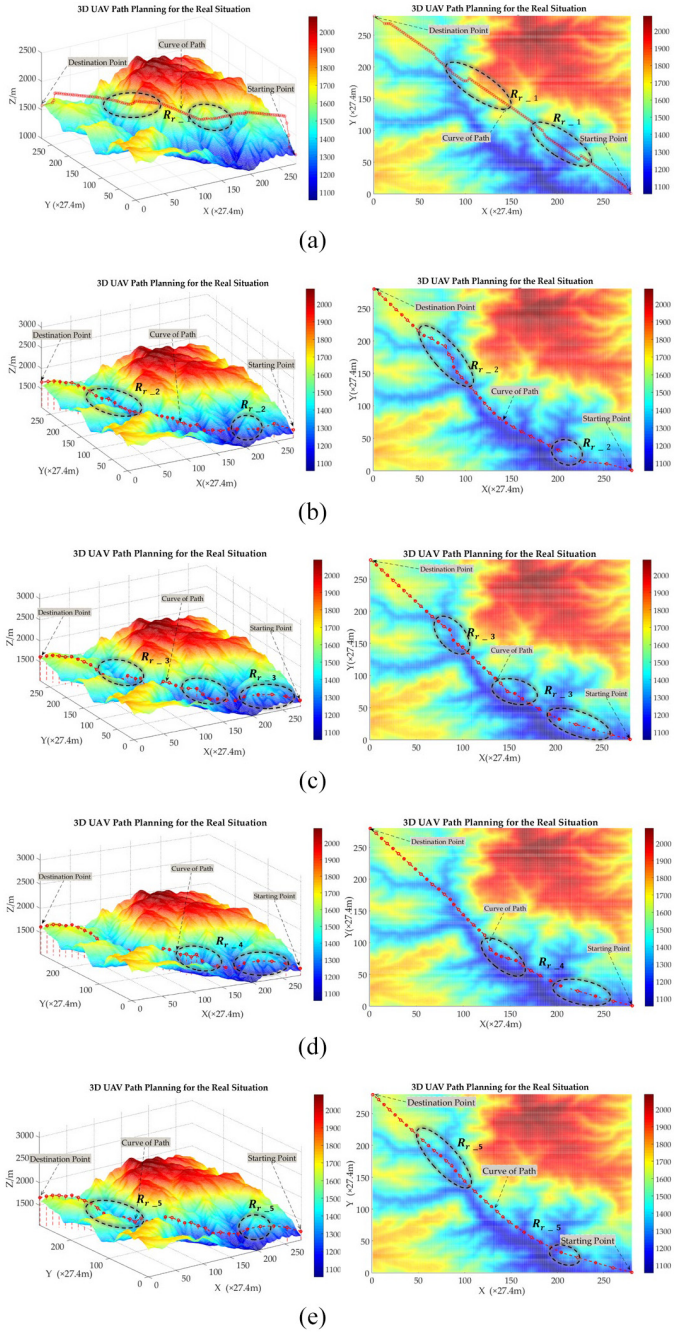

Fig. 16. Results for the real situation. (a) A*_real situation. (b) NSGA-II_real situation. (c) MOEA/D_real situation. (d) NSGA-III_real situation. (e) APPMS_real situation.

search capabilities, and effectively improves the optimization ability of individual solutions in the search population in the multidimensional and multimodal target space. Therefore, when optimizing the multiobjective 3-D path planning for a UAV in an actual environment, the Pareto front composed of the Pareto optimal solution set obtained by the proposed method has better values of HV, PD, and S. Thus, the effectiveness of the proposed APPMS path planning method has been further proved in this real-data experiment for a dam break emergency response scenario in a mining area. Thus, we can conclude that the proposed APPMS method has strong

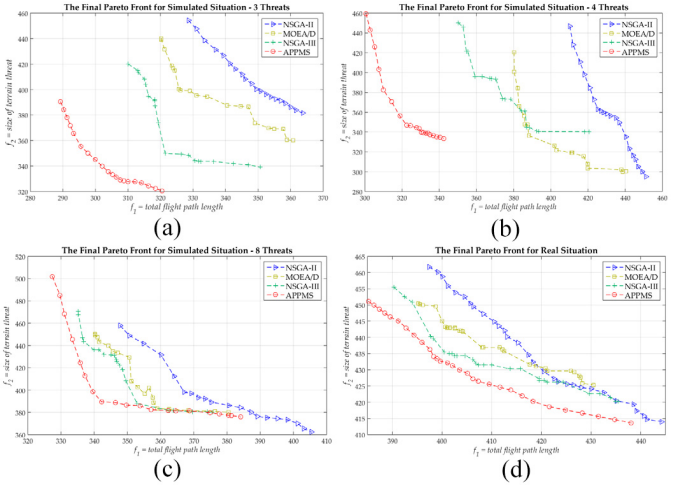

Fig. 17. Comparisons of the final Pareto fronts for the simulated and real-data experiments. (a) Three threats. (b) Four threats. (c) Eight threats. (d) Real situation.

practical application value, and could be used to provide effective decision making for UAV rapid response and flight control in emergency environments.

D. Analysis of the Computational Complexity and Time Cost

For the computational complexity of the proposed APPMS method, that is, Algorithm 1, we assume that the planned number of 3-D track points is n for a specific UAV path planning mission. Thus, the length of the solution individual is $l = 3 \times n$. The maximum number of iterations is $T_{\max}$, and the population size is P. The analysis of the computational complexity of the proposed method can be split into five main steps.

1) *Population Initialization:* The P solution individuals are initialized at the same time, for which the computational complexity is $O(P \times l)$.
2) *Reproduction:* The global and local search strategies are designed in this step, and assuming that the number of solution individuals in $N(t)$ is N_t, then the computational complexity is $O(N_t)$.
3) *Calculation of the Objective Functions:* The computational complexities for functions f_1 and f_2 are $\hbar = O(P \times l^2)$ and $\dot{\times} = O(P \times l^2 \times \theta^2)$, where $\theta = 3 \times n\_g$.
4) *Sorting and Updating:* The computational complexity of the Pareto ranking and density ranking are $O(2 \times P)$and $O(2 \times P \times \log(P))$.
5) *Main Loop:* There are $T_{\max}$ iterations for searching the UAV flight path, so the computational complexity is $O(T_{\max} \times P \times l^2 \times \theta^2)$.

For the actual time costs of the different UAV path planning methods, the comparison results are presented in Fig. 18. A personal computer equipped with eight central processing units (CPUs) (Intel Xeon CPU E3-1240 v6 @ 3.70 GHz) was used to conduct these experiments. It can be found that the traditional A* algorithm takes the least time, but with a poor effect. The MOEA/D method takes the most time, while the proposed APPMS method has a moderate computation time, while also obtaining the best performance.

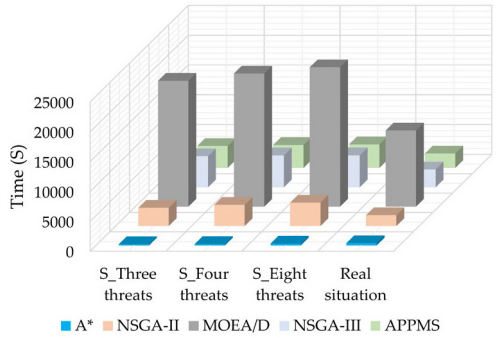

Fig. 18. Actual computation times of the different methods.

TABLE IV
RESULTS OF THE WILCOXON SIGNED-RANK TEST

Method	APPMS	NSGA-II	MOEA/D	NSGA-III
Simulated 3 threats		(+) (=) (+)	(+) (-) (+)	(+) (=) (+)
Simulated 4 threats		(+) (+) (-)	(-) (+) (-)	(=) (+) (-)
Simulated 8 threats		(+) (=) (+)	(+) (+) (=)	(+) (+) (+)
Real situation		(+) (+) (=)	(+) (+) (+)	(+) (+) (+)

E. Nonparametric Test

For the results of the multiobjective optimization-based methods, in order to better understand the performances, a nonparametric statistical significance test—the Wilcoxon signed-rank test—was used to evaluate the statistical significance of the results. The significance level was set to 0.05, and the test results are shown as (+), (−), or (=), respectively, when the proposed APPMS method is significantly better than, significantly worse than, or statistically equivalent to its peers. As shown in Table IV, for each comparison method, there are three columns of comparison results, representing HV, PD, and S, respectively. It can be found that the proposed APPMS method significantly outperforms the comparison methods in the simulated experiment with eight threats and the real-data experiment, which indicates that the proposed method can obtain a superior performance in more complex terrain environments. In addition, for the simulated experiments with three and four threats, the proposed method has more significant advantages, but it has disadvantages in some indicators, such as the indicator of S in the simulated experiment with four threats. Thus, overall, the proposed method performs significantly better than the other comparison methods.

V. CONCLUSION

In this article, in order to address the concerns in the practical UAV 3-D path planning task, an accurate UAV 3-D path planning method based on an improved multiobjective swarm intelligence algorithm has been presented (APPMS). In particular, an improved model for the objective functions and constraints has been creatively constructed for describing the flight distance and the degree of terrain threat. Moreover, a more effective search strategy has been designed, and in order to effectively search the 3-D path, a swarm intelligence search method based on improved ACO has also been designed. This method can keep the global and local search capabilities and ensure that the Pareto solution set keeps a uniform distribution and diversity, so that the final optimal solution can be better located. Furthermore, the superiority of the proposed method was confirmed in three sets of simulated digital terrain with three, four, and eight threats, and real DEM data for a simulated disaster emergency task, where the proposed APPMS method was compared with the traditional method of A* and the NSGA-II, MOEA/D, and NSGA-III-based multiobjective UAV 3-D path planning methods.

It is particularly important to design an effective UAV path planning algorithm for actual 3-D terrain scenarios. In future work, it will first be necessary to develop more effective search methods. Second, it will be necessary to simulate the constraints of actual flight conditions, to make the simulation closer to reality, such as the flight velocity of UAV. Third, it will be necessary to use more complex 3-D terrain data for UAV path planning testing, so as to promote rapid data collection and the subsequent decision making for emergency response scenarios in the future.

REFERENCES

[1] Y. Wang, Z.-Y. Ru, K. Wang, and P.-Q. Huang, "Joint deployment and task scheduling optimization for large-scale mobile users in multi-UAV-enabled mobile edge computing," *IEEE Trans. Cybern.*, vol. 50, no. 9, pp. 3984–3997, Sep. 2020.

[2] H. Liu, X. Li, M. Fan, G. Wu, W. Pedrycz, and P. N. Suganthan, "An autonomous path planning method for unmanned aerial vehicle based on a tangent intersection and target guidance strategy," *IEEE Trans. Intell. Transp. Syst.*, vol. 23, no. 4, pp. 3061–3073, Apr. 2022, doi: 10.1109/TITS.2020.3030444.

[3] H. Huang, A. V. Savkin, and C. Huang, "Reliable path planning for drone delivery using a stochastic time-dependent public transportation network," *IEEE Trans. Intell. Transp. Syst.*, vol. 22, no. 8, pp. 4941–4950, Aug. 2021, doi: 10.1109/TITS.2020.2983491.

[4] Z. Sun, G. G. Yen, J. Wu, H. Ren, H. An, and J. Yang, "Mission planning for energy-efficient passive UAV radar imaging system based on substage division collaborative search," *IEEE Trans. Cybern.*, early access, Aug. 3, 2021, doi: 10.1109/TCYB.2021.3090662.

[5] C. Ramirez-Atencia, G. Bello-Orgaz, M. D. R-Moreno, and D. Camacho, "Solving complex multi-UAV mission planning problems using multi-objective genetic algorithms," *Soft Comput.*, vol. 21, no. 17, pp. 4883–4900, 2017.

[6] J. Liu, W. Wang, T. Wang, Z. Shu, and X. Li, "A MOTIF-based rescue mission planning method for UAV swarms using an improved PICEA," *IEEE Access*, vol. 6, pp. 40778–40791, 2018.

[7] P. Petrides, P. Kolios, C. Kyrkou, T. Theocharides, and C. Panayiotou, "Disaster prevention and emergency response using unmanned aerial systems," in *Smart Cities in the Mediterranean*. Cham, Switzerland: Springer, 2017, pp. 379–403.

[8] R. Chai, A. Savvaris, A. Tsourdos, Y. Xia, and S. Chai, "Solving multiobjective constrained trajectory optimization problem by an extended evolutionary algorithm," *IEEE Trans. Cybern.*, vol. 50, no. 4, pp. 1630–1643, Apr. 2020.

[9] F. DuchoĖ *et al.*, "Path planning with modified a star algorithm for a mobile robot," *Procedia Eng.*, vol. 96, pp. 59–69, Dec. 2014.

[10] X. Yi, A. Zhu, S. X. Yang, and C. Luo, "A bio-inspired approach to task assignment of swarm robots in 3-D dynamic environments," *IEEE Trans. Cybern.*, vol. 47, no. 4, pp. 974–983, Apr. 2017.

[11] D. Feurer and F. Vinatier, "Joining multi-EPOCH archival aerial images in a single SfM block allows 3-D change detection with almost exclusively image information," *ISPRS J. Photogramm. Remote Sens.*, vol. 146, pp. 495–506, Nov. 2018.

[12] Y. Lin and S. Saripalli, "Sampling-based path planning for UAV collision avoidance," *IEEE Trans. Intell. Transp. Syst.*, vol. 18, no. 11, pp. 3179–3192, Nov. 2017.

[13] Y. V. Pehlivanoglu, "A new vibrational genetic algorithm enhanced with a Voronoi diagram for path planning of autonomous UAV," *Aerosp. Sci. Technol.*, vol. 16, no. 1, pp. 47–55, Jan./Feb. 2012.

[14] K. Yang, S. K. Gan, and S. Sukkarieh, "A Gaussian process-based RRT planner for the exploration of an unknown and cluttered environment with a UAV," *Adv. Robot.*, vol. 27, no. 6, pp. 431–443, Feb. 2013.

[15] S. Karaman and E. Frazzoli, "Incremental sampling-based algorithms for optimal motion planning," in *Robotics Science and Systems*. Cambridge, MA, USA: MIT Press, 2010, pp. 267–274.

[16] I. Noreen, A. Khan, and Z. Habib, "Optimal path planning using RRT* based approaches: A survey and future directions," *Int. J. Adv. Comput. Sci. Appl.*, vol. 7, no. 11, pp. 97–107, 2016.

[17] W. G. Aguilar, S. Morales, H. Ruiz, and V. Abad, "RRT* GL based optimal path planning for real-time navigation of UAVs," in *Proc. Int. Work Conf. Artif. Neural Netw.*, Jun. 2017, pp. 585–595.

[18] F. Yan, Y. S. Liu, and J. Z. Xiao, "Path planning in complex 3D environments using a probabilistic roadmap method," *Int. J. Autom. Comput.*, vol. 10, no. 6, pp. 525–533, May 2014.

[19] J. Wu, J. Yi, L. Gao, and X. Li, "Cooperative path planning of multiple UAVs based on pH curves and harmony search algorithm," in *Proc. IEEE 21st Int. Conf. Comput. Supported Cooperat. Work Design (CSCWD)*, Apr. 2017, pp. 540–544.

[20] F. L. L. Medeiros and J. D. S. Da Silva, "A Dijkstra algorithm for fixed-wing UAV motion planning based on terrain elevation," in *Proc. Braz. Symp. Artif. Intell.*, Oct. 2010, pp. 213–222.

[21] M. Chen, J. C. Shih, and C. J. Tomlin, "Multi-vehicle collision avoidance via Hamilton-Jacobi reachability and mixed integer programming," in *Proc. IEEE 55th Conf. Decis. Control (CDC)*, Dec. 2016, pp. 1695–1700.

[22] M. Radmanesh and M. Kumar, "Flight formation of UAVs in presence of moving obstacles using fast-dynamic mixed integer linear programming," *Aerosp. Sci. Technol.*, vol. 50, pp. 149–160, Mar. 2016.

[23] V. Roberge, M. Tarbouchi, and G. Labonté, "Fast genetic algorithm path planner for fixed-wing military UAV using GPU," *IEEE Trans. Aerosp. Electron. Syst.*, vol. 54, no. 5, pp. 2105–2117, Oct. 2018.

[24] J. D. S. Arantes, M. D. S. Arantes, C. F. M. Toledo, O. T. Júnior, and B. C. Williams, "Heuristic and genetic algorithm approaches for UAV path planning under critical situation," *Int. J. Artif. Intell. Tools*, vol. 26, no. 1, Feb. 2017, Art. no. 1760008.

[25] O. Zaki and M. Dunnigan, "A navigation strategy for an autonomous patrol vehicle based on multi-fusion planning algorithms and multi-paradigm representation schemes," *Robot. Auton. Syst.*, vol. 96, pp. 133–142, Oct. 2017.

[26] X. Liang, G. Meng, Y. Xu, and H. Luo, "A geometrical path planning method for unmanned aerial vehicle in 2D/3D complex environment," *Intell. Service Robot.*, vol. 11, no. 3, pp. 301–312, May 2018.

[27] C. Huang and J. Fei, "UAV path planning based on particle swarm optimization with global best path competition," *Int. J Pattern Recognit. Artif. Intell.*, vol. 32, no. 6, Jun. 2018, Art. no. 1859008.

[28] T. Hu, I. Ahmad, M. S. M. Alamgir, and K. Chang, "3D optimal surveillance trajectory planning for multiple UAVs by using particle swarm optimization with surveillance area priority," *IEEE Access*, vol. 8, pp. 86316–86327, 2020.

[29] U. Cekmez, M. Ozsiginan, and O. K. Sahingoz, "Multi colony ant optimization for UAV path planning with obstacle avoidance," in *Proc. Int. Conf. Unmanned Aircraft Syst. (ICUAS)*, Jun. 2016, pp. 47–52.

[30] H. Daryanavard and A. Harifi, "UAV path planning for data gathering of IoT nodes: Ant colony or simulated annealing optimization," in *Proc. 3rd Int. Conf. Internet Things Appl. (IoT)*, Apr. 2019, pp. 1–4.

[31] S. Mirjalili, S. M. Mirjalili, and A. Hatamlou, "Multi-verse optimizer: A nature-inspired algorithm for global optimization," *Neural Comput. Appl.*, vol. 27, no. 2, pp. 495–513, Feb. 2016.

[32] R. J. Szczerba, "Threat netting for real-time, intelligent route planners," in *Proc. IEEE Symp. Inf. Decis. Control*, Feb. 1999, pp. 377–382.

[33] A. N. Brintaki and I. K. Nikolos, "Coordinated UAV path planning using differential evolution," *Oper. Res.*, vol. 5, no. 3, pp. 487–502, Sep. 2005.

[34] Z. Sun, J. Wu, J. Yang, Y. Huang, C. Li, and D. Li, "Path planning for GEO-UAV bistatic SAR using constrained adaptive multiobjective differential evolution," *IEEE Trans. Geosci. Remote Sens.*, vol. 54, no. 11, pp. 6444–6457, Nov. 2016.

[35] Y. Zhao, Z. Zheng, and Y. Liu, "Survey on computational-intelligence-based UAV path planning," *Knowl. Based Syst.*, vol. 158, pp. 54–64, Oct. 2018.

[36] A. Bayrak and M. Ö. Efe, "FPGA based offline 3D UAV local path planner using evolutionary algorithms for unknown environments," in *Proc. 42nd Annu. Conf. IEEE Ind. Electron. Soc.*, Oct. 2016, pp. 4778–4783.

[37] X. Yang, M. Cai, and J. Li, "Path planning for unmanned aerial vehicles based on genetic programming," in *Proc. Chin. Control Decis. Conf.*, May 2016, pp. 717–722.

[38] L. Blasi, S. Barbato, and E. D'Amato, "A mixed probabilistic–geometric strategy for UAV optimum flight path identification based on bit-coded basic manoeuvres," *Aerosp. Sci. Technol.*, vol. 71, pp. 1–11, Dec. 2017.

[39] C. Huang *et al.*, "A new dynamic path planning approach for unmanned aerial vehicles," *Complexity*, vol. 2018, Nov. 2018, Art. no. 8420294.

[40] M. D. Phung, C. H. Quach, T. H. Dinh, and Q. Ha, "Enhanced discrete particle swarm optimization path planning for UAV vision-based surface inspection," *Autom. Construct.*, vol. 81, pp. 25–33, Sep. 2017.

[41] D. Adhikari, E. Kim, and H. Reza, "A fuzzy adaptive differential evolution for multi-objective 3D UAV path optimization," in *Proc. IEEE Congr. Evol. Comput. (CEC)*, Jul. 2017, pp. 2258–2265.

[42] X. Yu, C. Li, and J. F. Zhou, "A constrained differential evolution algorithm to solve UAV path planning in disaster scenarios," *Knowl. Based Syst.*, vol. 204, Sep. 2020, Art. no. 106209.

[43] B. Tong, L. Chen, and H. Duan, "A path planning method for UAVs based on multi-objective pigeon-inspired optimisation and differential evolution," *Int. J. Bio Inspired Comput.*, vol. 17, no. 2, pp. 105–112, Mar. 2021.

[44] Y. Wan, Y. Zhong, and A. Ma, "Fully automatic spectral–spatial fuzzy clustering using an adaptive multiobjective memetic algorithm for multispectral imagery," *IEEE Trans. Geosci. Remote Sens.*, vol. 57, no. 4, pp. 2324–2340, Apr. 2019.

[45] Y.-F. Ge *et al.*, "Distributed memetic algorithm for outsourced database fragmentation," *IEEE Trans. Cybern.*, vol. 57, no. 4, pp. 2324–2340, Apr. 2019, doi: 10.1109/TCYB.2020.3027962.

[46] M. Crepinšek, S. H. Liu, and M. Mernik, "Exploration and exploitation in evolutionary algorithms: A survey," *ACM Comput. Surveys*, vol. 45, no. 3, p. 35, Jun. 2013.

[47] X. Yu, C. Li, and J. Zhou, "A constrained differential evolution algorithm to solve UAV path planning in disaster scenarios," *Knowl. Based Syst.*, vol. 204, Sep. 2020, Art. no. 106209.

[48] J. Wu, Z. Peng, and J. Chen, "3D multi-constraint route planning for UAV low-altitude penetration based on multi-agent genetic algorithm," in *Proc. 18th World Congr. Int. Feder. Autom. Control Milano*, Jan. 2011, pp. 11821–11826.

[49] W. Li, L. He, and Y. Cao, "Many-objective evolutionary algorithm with reference point-based fuzzy correlation entropy for energy-efficient job shop scheduling with limited workers," *IEEE Trans. Cybern.*, early access, Apr. 19, 2021, doi: 10.1109/TCYB.2021.3069184.

[50] L. He, W. Li, Y. Zhang, and Y. Cao, "A discrete multi-objective fireworks algorithm for flowshop scheduling with sequence-dependent setup times," *Swarm Evol. Comput.*, vol. 51, Dec. 2019, Art. no. 100575.

[51] L. He, R. Chiong, W. Li, S. Dhakal, Y. Cao, and Y. Zhang, "Multiobjective optimization of energy-efficient job-shop scheduling with dynamic reference point-based fuzzy relative entropy," *IEEE Trans. Ind. Informat.*, vol. 18, no. 1, pp. 600–610, Jan. 2022, doi: 10.1109/TII.2021.3056425.

[52] G. Zhu, L. He, X. Ju, and W. Zhang, "A fitness assignment strategy based on the grey and entropy parallel analysis and its application to MOEA," *Eur. J. Oper. Res.*, vol. 265, no. 3, pp. 813–828, Mar. 2018.

[53] A. Colorni, M. Dorigo, and V. Maniezzo, "Distributed optimization by ant colonies," in *Proc. 1st Eur. Conf. Artif. Life*, 1991, pp. 134–142.

[54] M. Dorigo and L. M. Gambardella, "Ant colony system: A cooperative learning approach to the traveling salesman problem," *IEEE Trans. Evol. Comput.*, vol. 1, no. 1, pp. 53–66, Apr. 1997.

[55] W. Hong, K. Tang, A. Zhou, H. Ishibuchi, and X. Yao, "A scalable indicator-based evolutionary algorithm for large-scale multiobjective optimization," *IEEE Trans. Evol. Comput.*, vol. 23, no. 3, pp. 525–537, Jun. 2019.

[56] K. Deb, A. Pratap, S. Agarwal, and T. Meyarivan, "A fast and elitist multiobjective genetic algorithm: NSGA-II," *IEEE Trans. Evol. Comput.*, vol. 6, no. 2, pp. 182–197, Apr. 2002.

[57] X. Zhang, Y. Tian, and Y. Jin, "A knee point-driven evolutionary algorithm for many-objective optimization," *IEEE Trans. Evol. Comput.*, vol. 19, no. 6, pp. 761–776, Dec. 2015.

[58] G. Yu, Y. Jin, and M. Olhofer, "Benchmark problems and performance indicators for search of knee points in multiobjective optimization," *IEEE Trans. Cybern.*, vol. 50, no. 8, pp. 3531–3544, Aug. 2020.

[59] X. Zhou, X. Wang, and X. Gu, "Welding robot path planning problem based on discrete MOEA/D with hybrid environment selection," *Neural Comput. Appl.*, vol. 33, pp. 12881–12903, Apr. 2021.

[60] J. Liu, W. Wang, X. Li, T. Wang, S. Bai, and Y. Wang, "Solving a multi-objective mission planning problem for UAV swarms with an improved NSGA-III algorithm," *Int. J. Comput. Intell. Syst.*, vol. 11, no. 1, pp. 1067–1081, 2018.

[61] K. Shang and H. Ishibuchi, "A new hypervolume-based evolutionary algorithm for many-objective optimization," *IEEE Trans. Evol. Comput.*, vol. 24, no. 5, pp. 839–852, Oct. 2020, doi: 10.1109/TEVC.2020.2964705.
[62] H. Wang, Y. Jin, and X. Yao, "Diversity assessment in many-objective optimization," *IEEE Trans. Cybern.*, vol. 47, no. 6, pp. 1510–1522. Jun. 2017.
[63] J. R. Schott, "Fault tolerant design using single and multicriteria genetic algorithm optimization," DTIC, Fort Belvoir, VA, USA, Rep. CSDL-T-1251, 1995.

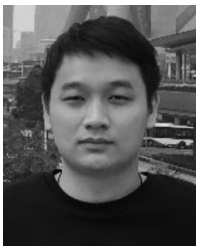

Yuting Wan (Student Member, IEEE) received the B.S. degree from the School of Geosciences and Info-Physics, Central South University, Changsha, China, in 2017. He is currently pursuing the Ph.D. degree in photogrammetry and remote sensing with the State Key Laboratory of Information Engineering in Surveying, Mapping and Remote Sensing, Wuhan University, Wuhan, China.

His major research interests include remote sensing image processing, evolutionary computation, multiobjective optimization, and neural architecture search.

Yanfei Zhong (Senior Member, IEEE) received the B.S. degree in information engineering and the Ph.D. degree in photogrammetry and remote sensing from Wuhan University, Wuhan, China, in 2002 and 2007, respectively.

Since 2010, he has been a Full professor with the State Key Laboratory of Information Engineering in Surveying, Mapping and Remote Sensing, Wuhan University. He organized the Intelligent Data Extraction, Analysis and Applications of Remote Sensing (RSIDEA) Research Group. He has published more than 100 research papers in international journals, such as *Remote Sensing of Environment*, *ISPRS Journal of Photogrammetry and Remote Sensing*, and IEEE TRANSACTIONS ON GEOSCIENCE AND REMOTE SENSING. His research interests include hyperspectral remote sensing information processing, high-resolution remote sensing image understanding, and geoscience interpretation for multisource remote sensing data and applications.

Dr. Zhong was a recipient of the 2016 Best Paper Theoretical Innovation Award from the International Society for Optics and Photonics (SPIE). He won the Second-Place Prize in 2013 IEEE GRSS Data Fusion Contest and the Single-View Semantic 3-D Challenge of the 2019 IEEE GRSS Data Fusion Contest, respectively. He is currently serving as an Associate Editor for the IEEE JOURNAL OF SELECTED TOPICS IN APPLIED EARTH OBSERVATIONS AND REMOTE SENSING and the *International Journal of Remote Sensing*. He is a Fellow of the Institution of Engineering and Technology.

Ailong Ma (Member, IEEE) received the B.S. degree from the China University of Petroleum, Qingdao, China, in 2010, and the Ph.D. degree in photogrammetry and remote sensing from Wuhan University, Wuhan, China, in 2017.

He is currently working as a Research Associate with Wuhan University. His major research interests are remote sensing image processing, evolutionary computing, and deep learning.

Liangpei Zhang (Fellow, IEEE) received the B.S. degree in physics from Hunan Normal University, Changsha, China, in 1982, the M.S. degree in optics from the Xi'an Institute of Optics and Precision Mechanics, Chinese Academy of Sciences, Xi'an, China, in 1988, and the Ph.D. degree in photogrammetry and remote sensing from Wuhan University, Wuhan, China, in 1998.

He is a "Chang-Jiang Scholar" Chair Professor appointed by the Ministry of Education of China, State Key Laboratory of Information Engineering in Surveying, Mapping, and Remote Sensing, Wuhan University. He was a Principal Scientist for the China State Key Basic Research Project from 2011 to 2016 appointed by the Ministry of National Science and Technology of China to lead the Remote Sensing Program in China. He has published more than 700 research papers and five books. He is the Institute for Scientific Information highly cited author. He is the holder of 30 patents. His research interests include hyperspectral remote sensing, high-resolution remote sensing, image processing, and artificial intelligence.

Dr. Zhang was a recipient of the 2010 Best Paper Boeing Award, the 2013 Best Paper ERDAS Award from the American Society of Photogrammetry and Remote Sensing, and the 2016 Best Paper Theoretical Innovation Award from the International Society for Optics and Photonics (SPIE). His research teams won the top three prizes of the IEEE GRSS 2014 Data Fusion Contest, and his students have been selected as the winners or finalists of the IEEE International Geoscience and Remote Sensing Symposium student paper contest in recent years. He also serves as an associate editor or editor of more than ten international journals. He is currently serving as an Associate Editor for the IEEE TRANSACTIONS ON GEOSCIENCE AND REMOTE SENSING. He is the Founding Chair of IEEE Geoscience and Remote Sensing Society Wuhan Chapter. He is a Fellow of the Institution of Engineering and Technology.